

Architectural Effects on Acid Reaction-Diffusion Kinetics in Molecular Glass Photoresists

Jing Sha,[†] Jin-Kyun Lee,[†] Shuhui Kang,[‡] Vivek M. Prabhu,^{*,‡} Christopher L. Soles,[‡] Peter V. Bonnesen,[§] and Christopher K. Ober^{*,†}

[†]Department of Materials Science and Engineering, Cornell University, Ithaca, New York 14853,

[‡]Polymers Division, National Institute of Standards and Technology, 100 Bureau Drive, Gaithersburg, Maryland 20899, and [§]Center for Nanophase Materials Sciences, Oak Ridge National Laboratory, Oak Ridge, Tennessee 37831

Received December 31, 2009. Revised Manuscript Received April 4, 2010

Understanding acid reaction-diffusion kinetics is crucial for controlling the lithographic performance of chemically amplified photoresists. In this work, we study how the molecular architectures of positive-tone chemically amplified molecular glass resists affect the acid reaction-diffusion kinetics during the post-expose bake (PEB) or annealing step. We compare the acid reaction-diffusion kinetics of a common photoacid generator in molecular glass resists with chemical similarity to poly(4-hydroxystyrene), and that are designed with branched and ring architectures. *In situ* Fourier transform infrared (FTIR) spectroscopy methods are used to measure reaction rate, acid trapping behavior, and acid diffusivity as a function of PEB temperature. We find that the acid reaction-diffusion kinetics in molecular glass resists is correlated to the film molar density that in turn depends on the architecture of the molecular glass molecules. These results allow modeling of the latent image formation in molecular glass resists that is critical for pattern feature resolution and line edge roughness. A comparison between experimentally measured and theoretically predicted diffusion lengths in one molecular glass resist system was made. Because little is understood of the fundamentals of acid diffusion in this class of molecular glass resists, this paper provides critical insight into the molecular design of next-generation photoresists for high-resolution lithography.

Introduction

Chemically amplified resists (CARs), a concept proposed by Ito, Willson, and Fréchet^{1,2} in 1982, are the current workhorse in photolithography for semiconductor device manufacturing because of their high sensitivity and good patterning performance. Irradiation activates photoacid generators (PAGs) in a CAR and the resulting photoacid molecules subsequently catalyze numerous reactions in a resist film before being trapped or quenched during the postexposure bake (PEB) step. These photoacids must be mobile enough within the CAR film to decompose a sufficient number of acid-labile protecting groups to achieve a solubility switch in the photoresist. However, excessive acid diffusion leads to image blur and resolution loss.^{3–6} Given the importance of this balance, measurements that quantify photoacid diffusion and the mechanisms of image blur and resolution are crucial to

optimize CAR photopatterning.^{7–13} Quantitative methods have been developed to measure photoacid diffusion using numerous strategies.^{11,14–23} Conventional CARs with polymer-based resist systems appear to have resolution

*Corresponding author. E-mail: cko3@cornell.edu (C.K.O.); vprabhu@nist.gov (V.M.P.).

- (1) Ito, H.; Willson, C.; Fréchet, J. *Digest of Technical Papers of the 1982 Symposium on VLSI Technology*; Sept 1–3, 1982; IEEE: Piscataway, NJ, 1982.
- (2) Ito, H.; Willson, C. *Polym. Eng. Sci.* **1983**, *23*, 331.
- (3) Ito, H. *Adv. Polym. Sci.* **2005**, *172*, 37–246.
- (4) Houle, F.; Hinsberg, W.; Sanchez, M.; Hoffnagle, J. *J. Vac. Sci. Technol., B: Microelectron. Nanometer Struct.* **2002**, *20*, 924.
- (5) Hinsberg, W.; Houle, F.; Sanchez, M.; Wallraff, G. *IBM J. Res. Dev.* **2001**, *45*, 667–682.
- (6) Wallraff, G.; Hinsberg, W. *Chem. Rev.* **1999**, *99*, 1801.

- (7) Goldfarb, D.; Angelopoulos, M.; Lin, E.; Jones, R.; Soles, C.; Lenhart, J.; Wu, W. *J. Vac. Sci. Technol., B: Microelectron. Nanometer Struct.* **2001**, *19*, 2699.
- (8) Stewart, M.; Tran, H.; Schmid, G.; Stachowiak, T.; Becker, D.; Willson, C. *J. Vac. Sci. Technol., B: Microelectron. Nanometer Struct.* **2002**, *20*, 2946.
- (9) Schmid, G.; Stewart, M.; Singh, V.; Willson, C. *J. Vac. Sci. Technol., B: Microelectron. Nanometer Struct.* **2002**, *20*, 185.
- (10) Hoffnagle, J.; Hinsberg, W.; Sanchez, M.; Houle, F. *Opt. Lett.* **2002**, *27*, 1776–1778.
- (11) Lin, E.; Soles, C.; Goldfarb, D.; Trinqué, B.; Burns, S.; Jones, R.; Lenhart, J.; Angelopoulos, M.; Willson, C.; Satija, S. *Science* **2002**, *297*, 372–375.
- (12) Kim, J.; Kim, Y.; Chon, S.; Nagai, T.; Noda, M.; Yamaguchi, Y.; Makita, Y.; Nemoto, H. *J. Photopolym. Sci. Technol.* **2004**, *17*, 379–384.
- (13) *International Technology Roadmap for Semiconductors 2007 Edition*, <http://www.itrs.net>, Lithography Section, p 10, 2007.
- (14) Kang, S.; Prabhu, V.; Wu, W.; Lin, E.; Choi, K.; Chandhok, M.; Younkin, T.; Yueh, W. *Proc. SPIE* **2009**, *7273*, 72733U.
- (15) Postnikov, S.; Stewart, M.; Tran, H.; Nierode, M.; Medeiros, D.; Cao, T.; Byers, J.; Webber, S.; Wilson, C. *J. Vac. Sci. Technol., B: Microelectron. Nanometer Struct.* **1999**, *17*, 3335.
- (16) Stewart, M.; Somervell, M.; Tran, H.; Postnikov, S.; Willson, C. *Proc. SPIE* **2000**, *3999*, 665–674.
- (17) Schnattinger, T.; Erdmann, A. *Proc. SPIE* **2008**, *6923*, 69230R.
- (18) Zuniga, M.; Neureuther, A. *J. Vac. Sci. Technol., B: Microelectron. Nanometer Struct.* **1995**, *13*, 2957.
- (19) Hinsberg, W.; Houle, F.; Sanchez, M.; Morrison, M.; Wallraff, G.; Larson, C.; Hoffnagle, J.; Brock, P.; Breyta, G. *Proc. SPIE* **2000**, *3999*, 148.

limits, such that critical dimensions (CD) of less than 22 nm may not be achieved. Because acid diffusion lengths are now approaching these CD values, acid diffusion remains critical to measure and control for the continued development of materials for next-generation patterning.

Recently, a new category of patterning materials, molecular glass (MG) resists, have attracted attention as an alternative to polymeric CARs because of their potential to improve line edge roughness (LER) and achieve smaller CD. MG resists are low-molar-mass, glass-forming organic materials and considered to have some advantages over linear polymers as photoresists. The small molecular size of MGs is believed to give a finer patterning “pixel” size to photoresists in comparison to their polymeric counterparts, which should enable high resolution patterning. This would be enabled by intimate mixing between PAG and molecular resist as determined by solid state nuclear magnetic resonance experiments on bulk blends.²⁴ Also, because the molecular glass resists have lower molecular mass, they are free of intermolecular entanglement, so less internal stress can build up during the development processes. Image distortion resulting from film stress is thereby reduced for MGs during pattern development. Despite these advantages, acid diffusion still occurs during the PEB step of chemically amplified MG resists and plays as important a role as in polymeric photoresists.^{25,26} In this study, we try to understand the photoacid-catalyzed reaction-diffusion kinetics in different types of MG resist materials for next-generation lithography.

MG resists investigated to date have structures including spiro,²⁷ ring,^{28–31} and branched architectures.³² In this work, we focus on four representative MG structures of both the ring and branched structures to investigate the effect of molecular architecture on acid reaction-diffusion kinetics. Two calix[4]resorcinarene derivatives^{29,31}

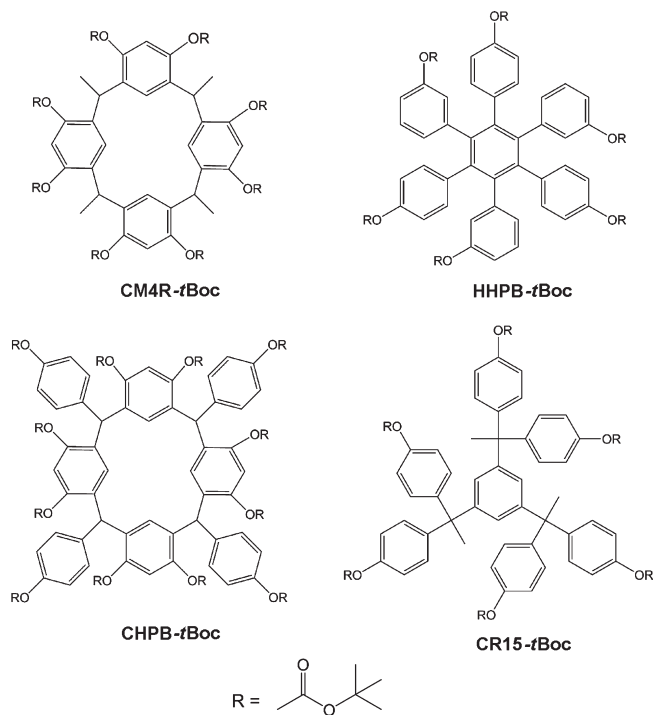


Figure 1. Chemical structures of the molecular glass resists studied in this work and the corresponding labels used to identify these compounds in this paper.

(**CM4R** and **CHPB**) and two phenolic MGs^{32,33} (**HHPB** and **CR15**) were fully protected with *tert*-butoxycarbonyl (*t*Boc) groups and used as the resist materials in this work (Figure 1). The MG resists possess structural similarity to novolac or poly(hydroxystyrene) (**PHOST**) based resists due to the incorporation of rigid phenyl rings. The glass-transition temperatures for these materials are between ≈ 80 °C and ≈ 90 °C in the bulk form, so processing temperatures among the MGs are not substantially different. As the *t*Boc groups are deprotected by acids during the post-exposure bake (PEB) step and the average degree of deprotection reaches a critical concentration, the MG resist film is transformed from insoluble to soluble in an alkaline developer (positive-tone development).

In this work, *in situ* FTIR methods are used to measure the *t*Boc group deprotection kinetics and therefore acid reaction-diffusion kinetics in exposed MG resist films during PEB.^{14,25,26} We have applied the strategy of using a bilayer film structure with a PAG-loaded MG resist layer on top of a PAG-free MG layer.^{14,25,26} This approach mimics an ideal lithographic line-edge that forms a well-defined step gradient of photoacids after flood ultraviolet (UV) light exposure. A soft-contact film transfer method using a poly(dimethylsiloxane) (PDMS) stamp was utilized for bilayer sample fabrication as described elsewhere^{14,25,26} (Figure 2a). This approach proved to be more convenient than double spin coating methods¹¹ which limit the use of the same spin-casting solvents and/or the same resist materials for both layers. Single layers of PAG-loaded MG resists were prepared, exposed and put on a preheated hot stage for *in situ* FTIR

- (20) Houle, F.; Hinsberg, W.; Morrison, M.; Sanchez, M.; Wallraff, G.; Larson, C.; Hoffnagle, J. *J. Vacuum Sci. Technol., B: Microelectron. Nanometer Struct.* **2000**, *18*, 1874.
- (21) Lavery, K.; Vogt, B.; Prabhu, V.; Lin, E.; Wu, W.; Satija, S.; Choi, K. *J. Vac. Sci. Technol., B: Microelectron. Nanometer Struct.* **2006**, *24*, 3044.
- (22) Vogt, B.; Kang, S.; Prabhu, V.; Lin, E.; Satija, S.; Turnquest, K.; Wu, W. *Macromolecules* **2006**, *39*, 8311–8317.
- (23) Vogt, B.; Kang, S.; Prabhu, V.; Rao, A.; Lin, E.; Wu, W.; Satija, S.; Turnquest, K. *J. Vac. Sci. Technol., B: Microelectron. Nanometer Struct.* **2007**, *25*, 175.
- (24) VanderHart, D.; Prabhu, V.; Silva, A.; Felix, N.; Ober, C. *J. Mater. Chem.* **2009**, *19*, 2683–2694.
- (25) Kang, S.; Lavery, K.; Choi, K.; Prabhu, V.; Wu, W.; Lin, E.; De Silva, A.; Felix, N.; Ober, C. *Proc. SPIE* **2008**, *6923*, 692317.
- (26) Kang, S.; Wu, W.; Choi, K.; De Silva, A.; Ober, C.; Prabhu, V. *Macromolecules* **2010**, accepted, DOI: 10.1021/ma902548a.
- (27) Dai, J.; Chang, S.; Hamad, A.; Felix, N.; Ober, C. *Chem. Mater.* **2006**, *18*, 3404–3411.
- (28) Ueda, M.; Takahashi, D.; Nakayama, T.; Haba, O. *Chem. Mater.* **1998**, *10*, 2230–2234.
- (29) (a) Young-Gil, K.; Kim, J.; Fujigaya, T.; Shibasaki, Y.; Ueda, M. *J. Mater. Chem.* **2002**, *12*, 53–57. (b) Cram, D. J.; Karbach, S.; Kim, H.-Y.; Knobler, C. B.; Maverick, E. F.; Ericson, J. L.; Helgeson, R. C. *J. Am. Chem. Soc.* **1988**, *110*, 2229–2237.
- (30) Ito, H.; Nakayama, T.; Sherwood, M.; Miller, D.; Ueda, M. *Chem. Mater.* **2008**, *20*, 341–356.
- (31) Chang, S.; Ayothi, R.; Bratton, D.; Yang, D.; Felix, N.; Cao, H.; Deng, H.; Ober, C. *J. Mater. Chem.* **2006**, *16*, 1470–1474.
- (32) De Silva, A.; Lee, J.; André, X.; Felix, N.; Cao, H.; Deng, H.; Ober, C. *Chem. Mater.* **2008**, *20*, 1606–1613.

- (33) Felix, N.; Tsuchiya, K.; Ober, C. *Adv. Mater.* **2006**, *18*, 442–446.

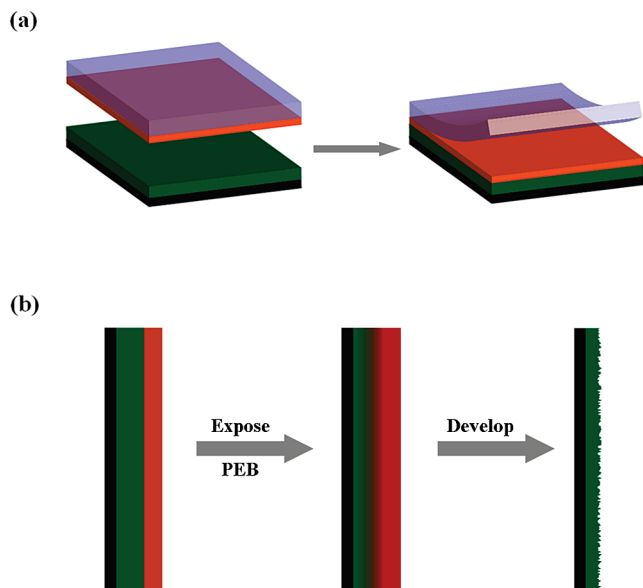


Figure 2. (a) Illustration of MG bilayer sample preparation: stamping PAG-loaded top layer (orange) onto PAG-free bottom layer (green) and peeling off PDMS stamp after the stack cools down. (b) Mimicking ideal exposure edge with a bilayer structure and processing of MG bilayer: exposure, PEB and development.

measurements. These experiments estimate the reaction kinetics constants (k_P and k_T) for each PEB temperature from the measured time dependent deprotection level ϕ . Subsequent *in situ* FTIR measurements on bilayer samples provide the diffusion coefficient (D_H) and the reaction kinetics constants (k_P and k_T) through simultaneous model fitting. Distinct reaction-diffusion kinetics performance was observed for each MG. Subsequently, the PEB bilayer samples were then developed in an aqueous base solution to determine the film thickness change and surface roughness of the bottom layers that relate to the CD and LER of MG resists in a true lithographic interface.

Experimental Section

Certain commercial equipment and materials are identified in this paper in order to specify adequately the experimental procedure. In no case does such identification imply recommendations by the National Institute of Standards and Technology nor does it imply that the material or equipment identified is necessarily the best available for this purpose.

Materials. 1,3,5-Triacetylbenzene was purchased from TCI America and used as received. 4-Hydroxybenzaldehyde, resorcinol, aldehyde, BBr_3 (1 M solution in dichloromethane), 3-iodoanisole, triphenylsulfonium perfluoro-1-butanefluoroborate (TPS-PFBS), anhydrous tetrahydrofuran (THF), and propylene glycol monomethyl ether acetate (PGMEA) were purchased from Sigma-Aldrich and used without further purification. 4-Ethynylanisole and $Co_2(CO)_8$ were purchased from AlfaAesar and used as received. Di-*tert*-butyl dicarbonate was purchased from either Fluka or Aldrich and used as received. Dioxane was dried over Na/benzophenone and distilled under reduced pressure. Commercially available AZ 300 MIF was employed as the developer (0.26 N tetramethylammonium hydroxide in water, TMAH). Sylgard 184 silicone elastomer kit was purchased from Dow Corning and used to make polydimethylsiloxane (PDMS) stamps.

Synthesis of Molecular Glass Photoresists. Tetra-*C*-methylcalix[4]resorcinarene (**CM4R**),²⁹ *C*-4-hydroxyphenylcalix[4]resorcinarene (**CHPB**),³¹ hexa-(3 or 4-hydroxyphenyl)benzene (**HHPB**),³³ 1,3,5-tri(1,1-di(4-hydroxyphenyl)ethyl)benzene (**CR15**),³² and their fully *tert*-butoxycarbonyl (*t*Boc)-protected molecular glass resists were prepared according to the procedures in the literature. The compounds were characterized by proton and carbon NMR, and chemical shifts were consistent with those reported in the literature.

Of specific note, the parent resorcinarene compound, (**CM4R**), was synthesized following literature procedures and purification methods known to afford the pure all *cis* or "*ccc'*" isomer (which is the cup-shaped isomer.) Our 1H and ^{13}C NMR spectral data on the tetra-*C*-methylcalix[4]resorcinarene were in agreement with the literature NMR spectral data^{29a} in the manuscript reported for the *ccc* isomer as well as the NMR data of ref 30. Because the parent **CM4R** is all *cis*, the *t*Boc derivatives will also be all *cis*. On the other hand, the parent **CHPB** was not purified as **CM4R** and is believed to be a mixture of *cis* and *trans* isomers.

Sample Preparation. Single layers and bilayers of each MG resist were prepared. Resist solutions were used containing 3–5% by mass MG in PGMEA. The photoacid generator, TPS-PFBS, was added to the solution at a concentration of 5% by mass of the MG for both the single-layer samples and the top layer of the bilayer samples. For single-layer samples, solutions of MG resist and TPS-PFBS were spin-cast on Au-coated silicon substrates at 2000 rpm (209 rad/s) and post-apply baked at 90 °C for 60 s. The final film thicknesses were generally 50 nm to 100 nm depending on the resist mass fraction. A PDMS stamping technique^{25,26} was used to create MG resist bilayers with PAG-loaded resist films at the top and PAG-free films at the bottom. The bottom layers of bilayer samples were prepared on Au-coated silicon substrates from PAG-free solutions in the same way as single-layer samples. Resist solutions containing PAG were spin-cast on PDMS substrates and then stamped onto prepared PAG-free resist films at 75 °C for 20 s. PDMS stamps were peeled off after the stacks cooled down. The resist bilayers were baked again at 75 °C for 60 s to remove residual solvents.

Exposure and Development. An Oriel UV exposure system was used for the reaction kinetics studies at a dose of ≈ 250 mJ/cm² with 248 nm broadband radiation. The samples prepared for additional development and AFM characterization were exposed with an ABM contact aligner at a dose of ≈ 250 mJ/cm² with 254 nm. At these exposure doses, all the photoacid generators were activated, so the initial acid concentration may be calculated using the molecular masses of the resist components. After PEB, bilayer samples were developed in a commercial developer AZ 300 MIF for 60 s, rinsed with deionized water, and blown dry with N_2 .

Characterization. Thermogravimetric analysis was performed using a TA 500 TGA with a heating rate of 10 °C/min under a dry N_2 atmosphere. Glass-transition temperatures (T_g) were measured on a TA 1000 DSC using repeated heat/cool cycles at 10 °C/min between -50 °C and 130 °C. MG resist film thicknesses were measured with a J.A. Woollam IR spectroscopic ellipsometer. All the Fourier transform infrared (FTIR) spectra were collected using polarization-modulation infrared reflection-absorption spectroscopy (PM-IRRAS) at 8 cm⁻¹ resolution on exposed resist films. Silicon wafers coated with 100 nm thick Au were used as substrates for MG samples to increase IR reflectivity in all measurements and mounted on a preheated hot stage through vacuum contact. The uncertainty in deprotection quantification is ≈ 0.01 – 0.02 . X-ray reflectivity measurements were carried out on a Philips X'Pert MRD

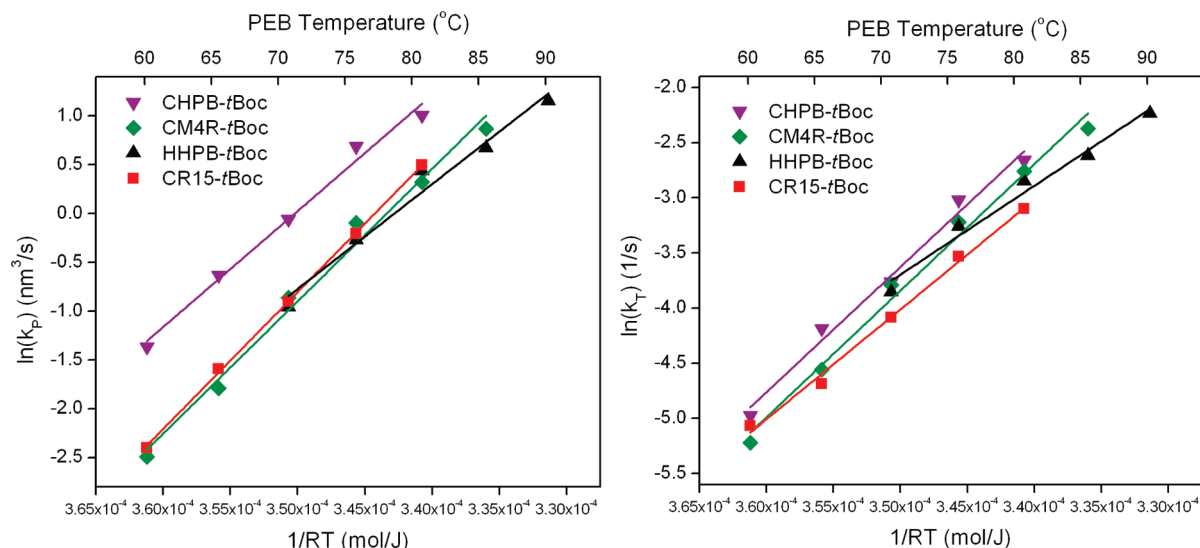


Figure 3. (a) Reaction rate constants k_p and (b) acid trapping rate constants k_T for the systems of TPS-PFBS and the four molecular glasses at varying PEB temperatures. The solid lines are fitted curves from Arrhenius model.

diffractometer with fine focus X-ray tubes with a wavelength of 1.54 Å. Atomic force microscopy (AFM) was performed on developed bilayer samples with a Veeco Dimension 3100 in tapping mode.

Results and Discussion

A reaction model^{25,26} was used to describe the acid-catalyzed deprotection and the acid diffusion/trapping during the PEB (eqs 1 and 2). In the differential equations, H is the acid concentration and ϕ is deprotection level of the MG resist that was quantified by the C=O stretching vibrational spectroscopic band around 1760 cm⁻¹. The reaction rate constant (k_p), the trapping rate constant (k_T) and the acid diffusion coefficient (D_H) are the three kinetic parameters that were measured and compared in this study. The relationship between the initial acid concentration H and PAG loading concentration ([PAG]), Dill's parameter (C) and the exposure dose (E) can be described as $H = [\text{PAG}](1 - e^{-CE})$. Because we exposed all the PAG-loaded MG resist films at high doses and essentially all the PAGs were activated, the initial acid concentration H is considered the same as the PAG loading concentration.

$$\frac{\partial \phi}{\partial t} = k_p H (1 - \phi) \quad (1)$$

$$\frac{\partial H}{\partial t} = D_H \nabla^2 H - k_T H \phi \quad (2)$$

Single layers of PAG-loaded MG resists were prepared and exposed using a sufficiently high exposure dose of UV light to activate all the photoacid generators in the films. Immediately following exposure, sample films were placed on the preheated hot stage of the FTIR spectrometer for *in situ* measurement of deprotection levels of *t*Boc groups. From the time-dependent deprotection level $\phi(t)$, the reaction rate constant k_p and acid trapping rate

constant k_T were estimated by the model for each PEB temperature.

The exposure and measurement conditions for the bilayer samples were the same as those used for the single layers. In the bilayer samples, the acids generated in the top layer deprotect the MG resist molecules in the neighboring regions and further diffuse into the PAG-free bottom layer during PEB. The time-dependent deprotection level ϕ of the bilayer samples is fit simultaneously to obtain k_p , k_T , and the acid diffusion coefficient D_H .

The resulting reaction rate constants and acid trapping rate constants for PEB temperatures varying from 60 to 90 °C are shown in panels a and b in Figure 3, respectively, for TPS-PFBS PAG with the four MG resists. The **CM4R-*t*Boc**, **HHPB-*t*Boc**, and **CR15-*t*Boc** systems show no substantial differences in the reaction rate constants while those for **CHPB-*t*Boc**/TPS-PFBS are significantly higher. The reaction rate constants increase with PEB temperature for each MG resist. Because the PEB temperatures are all below T_g , the temperature dependence of k_p can be described by an Arrhenius equation, $\ln(k_p) = A - E_a/RT$, where E_a is the activation energy, A is a prefactor, T is PEB temperature, and R is the universal gas constant. The fitted A and E_a values of the reaction constants of all resist systems are summarized in Table 1, with uncertainty estimated as one standard deviation from the mean. The acid trapping rate constants k_T do not differ significantly among the resist systems as a function of temperature, whereas significant and systematic differences in acid diffusivity were observed among different MG architectures. Figure 4 shows the acid diffusion coefficients in all the MG resist systems at the different PEB temperatures. The acid diffusivity D_H is the lowest in **HHPB-*t*Boc**, moderate in **CR15-*t*Boc** and **CM4R-*t*Boc**, and the highest in **CHPB-*t*Boc**. The temperature dependence of both k_T and D_H also follow the Arrhenius equations with prefactors A and activation energies E_a summarized in Table 1.

Table 1. Summary of Fitted Prefactors A and Activation Energies E_a for k_P , k_T , and D_H of TPS-PFBS in the MG Resists

	reaction rate constant k_P		acid trapping constant k_T		diffusion coefficient D_H	
	A	E_a (kJ/mol)	A	E_a (kJ/mol)	A	E_a (kJ/mol)
CHPB- <i>t</i> Boc	42 ± 2	112 ± 7	36 ± 2	114 ± 7	33 ± 2	91 ± 5
CM4R- <i>t</i> Boc	47 ± 3	136 ± 7	36 ± 2	115 ± 6	44 ± 2	125 ± 7
HHPB- <i>t</i> Boc	37 ± 3	107 ± 10	25 ± 2	81 ± 7	41 ± 4	125 ± 11
CR15- <i>t</i> Boc	48 ± 1	140 ± 2	31 ± 1	100 ± 4	44 ± 3	127 ± 8

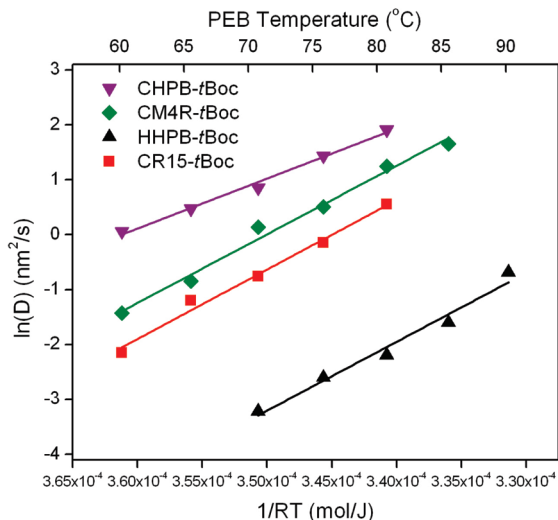


Figure 4. Diffusion coefficients of TPS-PFBS in the four molecular glass resists at various PEB temperatures. The solid lines are fitted curves from Arrhenius model.

Because all the *in situ* FTIR measurements were conducted below the T_g of the MGs, the transport process was expected to follow an Arrhenius dependence and it should depend on the mass density, packing and free volume in the MGs. The mass density of the thin films was measured by X-ray reflectivity from the critical-edge region (Table 2) using MG films without any additives. The mass density was converted to molar density using the known chemical composition. The trend of molar densities is $\text{HHPB-}t\text{Boc} > \text{CR15-}t\text{Boc} > \text{CM4R-}t\text{Boc} > \text{CHPB-}t\text{Boc}$, which shows an opposite trend to the acid diffusivity in the studied MG resist systems ($\text{HHPB-}t\text{Boc} < \text{CR15-}t\text{Boc} < \text{CM4R-}t\text{Boc} < \text{CHPB-}t\text{Boc}$). This observation follows concepts provided by free volume theory,³⁴ such that the more free volume present in a resist film, the more freely acid molecules can “hop” and diffuse. Free volumes in resist films can be experimentally inferred from mass/molar densities. According to energy minimization modeling using the MM2 method, all the MG molecules in this study are individually estimated to be approximately 2 nm in size. Therefore, a higher molar density can be translated into less free volume in the resist system or closer packing of resist molecules. For example, the relative planarity of $\text{HHPB-}t\text{Boc}$ molecules can contribute to a denser packing configuration while $\text{CHPB-}t\text{Boc}$ and $\text{CM4R-}t\text{Boc}$ molecules are ring-shaped and may leave more voids among resist molecules such as within the calix[4]resorcinarene cavity and as a result are less dense.

The protecting group concentrations can also be calculated by multiplying MG molar densities with the number of protecting groups per molecule. With a higher density of protecting groups, there are more hydroxyl groups per unit volume after deprotection. Therefore, this increases the probability that the photoacids interact with the hydroxyl groups and become trapped instead of moving on to deprotect more *t*Boc groups. The trapping constants in Figure 3b appear clustered but there is a noticeable trend at each PEB temperature: $k_T(\text{CHPB-}t\text{Boc}) > k_T(\text{CM4R-}t\text{Boc}) > k_T(\text{CR15-}t\text{Boc})$, which is consistent with the trend in protecting group concentrations (Table 2): $\text{CHPB-}t\text{Boc} > \text{CM4R-}t\text{Boc} > \text{CR15-}t\text{Boc}$. A crossover between $k_T(\text{HHPB-}t\text{Boc})$ and $k_T(\text{CM4R-}t\text{Boc})$ was observed and the difference in k_T cannot be explained just by protecting group concentrations. There may be additional mechanisms dominating in the case of $\text{HHPB-}t\text{Boc}$ but it is not clear at the moment.

From the above results, we can see that the acid diffusivities in the MG resist systems show apparent variances whereas the reaction and trapping processes are not widely different. Therefore, the choice of a MG resist system may not be able to control reactivity but only acid diffusivity. Both acid reactivity and diffusivity in CARs are required, however, to control latent image and resolution. Therefore, we demonstrate such effects with reaction-diffusion kinetics modeling in one resist system and compare with the experimental diffusion lengths determined by the difference in film thickness before and after development.

In another set of experiments, separate sets of bilayer samples were exposed and postexposure baked at 75 °C for 30, 60, 120, and 180 s and then developed with AZ 300 MIF. A representative result of the thickness loss and surface roughness for $\text{CR15-}t\text{Boc}$ bottom layer are plotted in Figure 5. As the PEB time increased, more photoacids diffused from the top to the bottom layer resulting in a higher deprotection level of *t*Boc groups in the bottom layer and thus larger film thickness loss after development. The experimental diffusion length, which is the difference between the initial bottom layer thickness and final developed thickness, were measured to be 1.3, 8.7, 9.8, and 13.7 nm as PEB time increases from 30 to 180 s. The measured surface root-mean-square (rms) roughness of the developed bottom layer dropped to the lowest value of 1.42 nm (PEB time of 120 s) and slightly increased to ca. 1.80 nm at 180 s of PEB.

The reaction-diffusion process in the $\text{CR15-}t\text{Boc}$ resist system was simulated with the kinetic model mentioned earlier using the measured parameters (k_P , k_T , D_H) at a PEB temperature of 75 °C (Figure 6). The deprotection level of $\text{CR15-}t\text{Boc}$ was measured to be 37.5% for

(34) Crank, J.; Park, G. *Diffusion in Polymers*; Academic Press, 1968.

Table 2. Mass and Molar Densities and Protecting Group Concentrations of Molecular Glass Resist Thin Films

	CHPB- <i>t</i> Boc	CM4R- <i>t</i> Boc	HHPB- <i>t</i> Boc	CR15- <i>t</i> Boc
mass density (g/cm ³)	1.117	1.092	1.124	1.114
molar density (mol/cm ³)	5.427×10^{-4}	8.116×10^{-4}	9.128×10^{-4}	8.468×10^{-4}
protecting group concentration (nm ⁻³)	3.922	3.910	3.298	3.060

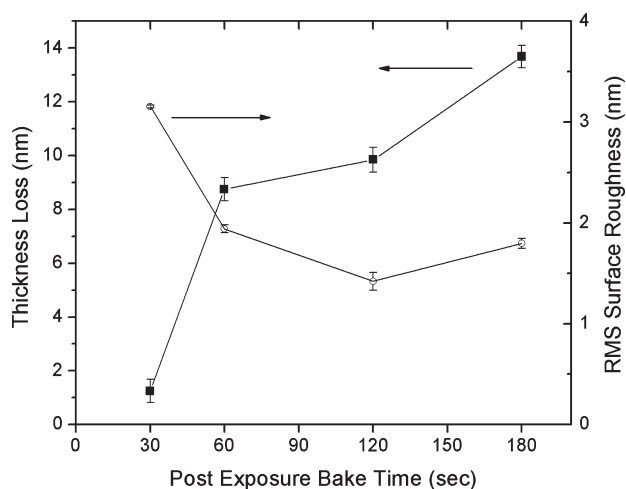


Figure 5. Resist film thickness loss (solid squares) and surface roughness (open circles) of the bottom layer of a **CR15-*t*Boc** bilayer sample after development. The change in film thickness, or thickness loss, is a measure of the acid diffusion length (L_d).

solubility switching to occur and thus the simulated diffusion length was determined to be 1.5, 5, 9, and 11 nm, respectively, for 30–180 s of PEB, which shows excellent agreement with the experimental data. On the other hand, the slope of the diffusion front shows a monotonic decrease as PEB time increases while the experimental surface roughness shows a slight minimum at PEB time of 120 s. A recent theoretical study showed that post-development LER of the exposure edge is inversely proportional to the latent image log slope (LILS),³⁵ thus a larger deprotection level gradient at the solubility switch corresponds to lower surface roughness of the developed bottom layer. The measured surface roughness of **CR15-*t*Boc** does not agree with the trend of deprotection level gradient at the solubility switch, although the differences are small. In this case, the ideal model does not fall within the experimental data. However, there are many aspects that remain critical for final roughness, such as chemical composition heterogeneity²⁰ and development mechanism.

Previous efforts using AFM images of latent images of 13.5 nm extreme-ultraviolet light (EUV) exposed polymer and **CM4R** photoresists show topographic features related to the deprotection level of the resist. Comparison of latent image LER for a polymeric and molecular glass (**CM4R**) photoresist with identical photoacid generator exhibited similar dependence on the deprotection gradient. The latent images of features as small as 20 nm were clearly resolved by AFM over a wide range of exposures despite these features not appearing after development.³⁶ Therefore, development

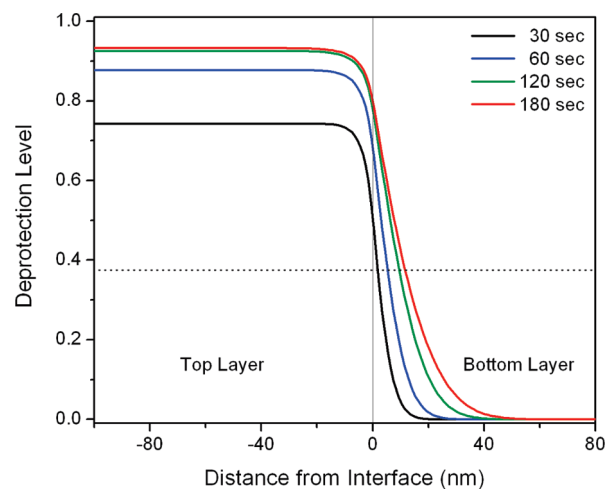


Figure 6. Calculated deprotection profile of **CR15-*t*Boc** at 75 °C PEB temperature for various PEB times. The dotted line marks the deprotection level at solubility switch of CR15 in the developer.

process and development contrast should be an area of increased attention; perhaps this is a future role of negative-tone development with molecular resists.

Conclusion

We have demonstrated a detailed study of acid reaction-diffusion kinetics behavior of four MG photoresists. Although reactivity and trapping of acids did not show significant differences among the MG resist systems, acid diffusivity varied systematically with resist architecture and molar density. Photoacids generated in the ring-shaped **CHPB-*t*Boc** resist system was found to have both the highest reactivity and the highest acid diffusivity compared to the other MG resists used in this study. A higher reaction rate is beneficial because for a given PEB time, it enables a larger extent of deprotection to occur that favors increased trapping; therefore, **CHPB-*t*Boc** did not show patternability inferior to the other MG resists.³⁷ We have also provided a hypothesis of how molecular architectures of the MGs impact acid kinetics during PEB. This study is the first attempt at a comprehensive characterization of structurally different MG resists with predictions of their lithographic performance.

Acknowledgment. The authors acknowledge Cornell Nano-scale Science and Technology Facility (CNF) and Cornell Center for Materials Research (CCMR) for use of facilities. The National Science Foundation (Grant DMR-0518785) is acknowledged for partial support of this work. The portion of this research carried out at Oak Ridge National Laboratory's Center for Nanophase Materials Sciences was sponsored by the Scientific User Facilities Division, Office of Basic Energy Sciences, U.S. Department of Energy.

(35) Bristol, R. Proceedings of SPIE, **2007**; 6519, p 65190W.

(36) Woodward, J. T.; Choi, K. W.; Prabhu, V. M.; Kang, S.; Lavery, K. A.; Wu, W. I.; Leeson, M.; De Silva, A.; Felix, N. M.; Ober, C. K. Proceeding of SPIE, **2008**, 6923, pp 69232B-12.

(37) De Silva, A.; Felix, N.; Ober, C. *Adv. Mater.* **2008**, 20, 3355–3361.